
Article:
Zhao, J orcid.org/0000-0002-8714-7798, Yao, G, Ramisetti, S orcid.org/0000-0002-2927-5257 et al. (2 more authors) (2019) Molecular dynamics investigation of substrate wettability alteration and oil transport in a calcite nanopore. Fuel, 239. pp. 1149-1161. ISSN 1873-7153

https://doi.org/10.1016/j.fuel.2018.11.089

Molecular dynamics investigation of substrate wettability alteration and oil transport in a calcite nanopore

Jin Zhao [a], Guice Yao [a], Srinivasa B. Ramisetti [a], Robert B. Hammond [a], Dongsheng Wen [b,a *]

[a]School of Chemical and Process Engineering, University of Leeds, Leeds, LS2 9JT, UK

[b]School of Aeronautic Science and Engineering, Beihang University, 100191, Beijing, P. R. China

Abstract

Low salinity flooding has been proposed as a promising method for enhanced oil recovery, but the underlying mechanism remains unclear especially for carbonate reservoirs. This work investigates the effect of water salinity in altering the wettability of nano-slit pores for three types of calcite surfaces (i.e., a neutral nonpolar $\{10\bar{1}4\}$ surface, and the polar {0001} surface with positively and negatively charged surfaces) using classical, equilibrium molecular dynamic (EMD) simulations. In addition, non-equilibrium MD simulations (NEMD) reveal the influence of wettability on the oil transport properties in a nano-pore at different salt concentrations of sodium chloride (NaCl) (0.20 M, 0.50 M, and 1.00 M). Results show that increasing water salinity has little effect on the wettability of a nano-pore comprised of neutral calcite surfaces. For a calcite nano-slit pore comprised of charged surfaces, however, the dipole-ion interaction alters the surface wettability creating a more hydrophilic surface due to the hydration effect of ions at elevated salt concentrations. While a partially decane-wet neutral nonpolar calcite surface

greatly inhibits the movement of an oil droplet in the pore, greater oil mobility is achieved for dipolar nano-pores, especially at elevated salt concentrations.

Keywords

Molecular Dynamics, Enhanced Oil Recovery, Low Salinity, Wettability, Dipolar nano-pores

1. Introduction

Low-salinity water flooding has been of interest as a promising method for enhanced oil recovery (EOR) [1]. A number of laboratory and field studies have shown that use of low-salinity water injection could modify the substrate wettability and increase oil recovery rate in sandstone reservoirs [2, 3]. Understanding the wettability of mineral surfaces is crucial not only for EOR from conventional and non-conventional oil fields, but also for the geological sealing of oil and gas by cap rocks [4, 5]. Though there is general agreement that the EOR effect by low-salinity water flooding is related to modification of substrate wettability creating more hydrophilic surfaces, the underpinning mechanism leading to wettability change is still a matter of debate [6-9].

It has been noted that the observed low-salinity EOR effects have been mainly for sandstone reservoirs containing clay minerals, where organic materials initially adsorbed on the clay may be desorbed due to an increase in pH caused by the desorption of active ions in the presence of low salinity [10-12]. In addition, a number of mechanisms such as sweep-efficiency improvement, interfacial tension (IFT) reduction, multi-component ionic exchange, and electrical double layer (EDL) expansion [13, 14] have been proposed to explain the wettability alteration. However, the low-salinity effect in carbonate rocks, the largest share in reservoirs, has been less

explored and the results are very contradictory [15, 16]. It has been shown experimentally that the effects of salinity on carbonates are quite different to those on sandstone cores [17-19]. The rock minerology, especially the presence of anhydrite in carbonate rocks, could affect the low salinity effect significantly [20-24]. The effect of multiple-component ionic exchange between adsorbed oil components, cations in the salt water and mineral surfaces has been proposed [25, 26], and the effect of IFT reduction was found to be too small to explain the experimental results [27-29].

It is believed that controversies relating to experimental observations of the low-salinity effect are caused, mainly, by the complexities of oil components, the water environment and the minerology of reservoir rocks. From the perspective of design of experiments, many of the key process parameters are closely interrelated making it very challenging to change one while keeping others unchanged, which in turn makes identification of the mechanism difficult. With rapid advances in high-performance computers and continuous development of force field potentials in the last few decades, molecular dynamics (MD) simulation has been widely used to investigate the complicated interactions between minerals, water, and organic materials at the atomic level. For instance, Wang et al. [30-32] investigated oil droplet detachment from virtual solid surfaces and demonstrated wettability alteration by charged hydrophobic nanoparticles, leading to highly efficient removal of oil droplets from solid surfaces. Underwood et al. [33-35] carried out MD simulations of oil detachment from clay surfaces and discussed three mechanisms related to low-salinity flooding, namely EDL expansion, multi-component ionic exchange and pH effects. Zhang et al. [36] simulated the interactions between clay minerals and confined pore fluids and showed that the salt ions adsorption onto clay surfaces could promote surface hydrophilicity. These studies have advanced our understanding of the low salinity effect

from an atomistic perspective for clay sandstones, whereas an understanding for carbonate rocks remains very limited.

Under ambient conditions calcite is the most stable polymorph of calcium carbonate ($CaCO_3$), and calcite minerals are a dominant component of rocks in oil reservoirs [37]. The surface properties of calcite are not stationary as adsorption/desorption of ions occurs constantly between the surface and the fluid inclusions [38]. For calcite, the $\{10\bar{1}4\}$ surface is the most stable surface in both vacuum and aqueous environment, and has little effective charge on the surface, hence, this is the surface considered for the MD simulations in this work. Meanwhile, solid surfaces in a nonconventional petroleum reservoir include both kerogen and mineral surfaces, which may be either polar or nonpolar. And in particular most mineral surfaces have polar character [39]. Therefore, the calcite {0001} surface is chosen in this work to examine the dipolar pore effect on the low-salinity EOR performance. The form {0001} of calcite has been found its occurrence frequency near 17% in natural samples grown from solution through statistical studies by Goldsmith and Sunagawa [40], which is a rather astonishing feature for a kinked/twinning face. As a common twinning plane, the calcite {0001} surface can be terminated in two ways, either by a layer of calcium atoms with positive charges, or carbonate groups with negative charges.

The polarizability of calcite mineral surfaces could affect strongly the interactions at the oil/brine/rock interface, which may be one of the reasons for the contradictory results reported for carbonate rocks [17-25]. Calcite $\{10\bar{1}4\}$ and {0001} surfaces are selected in this work as representative mineral surfaces of nano-pore walls with neutral and charged characteristics. The effects of surface charge in altering the wettability of calcite mineral surfaces, in the presence of different salt concentrations, are investigated using classical, equilibrium MD simulation (EMD)

methods. In addition, the impact of changes in wettability on the hydrodynamics of the water/n-decane/salts fluids confined in calcite nano-pores during the flooding process are investigated using the Non-Equilibrium MD simulation (NEMD) method.

2. Methodology

2.1 Model Construction

The initial configurations for the simulation models, as illustrated in Figure 1, were generated using the Material Studio (MS) package [41]. Each simulation system was composed of two parts namely, an immobile (solid) part consisting of nano-slit pore walls and a mobile (fluid) part consisting of a salt/water/oil mixture.

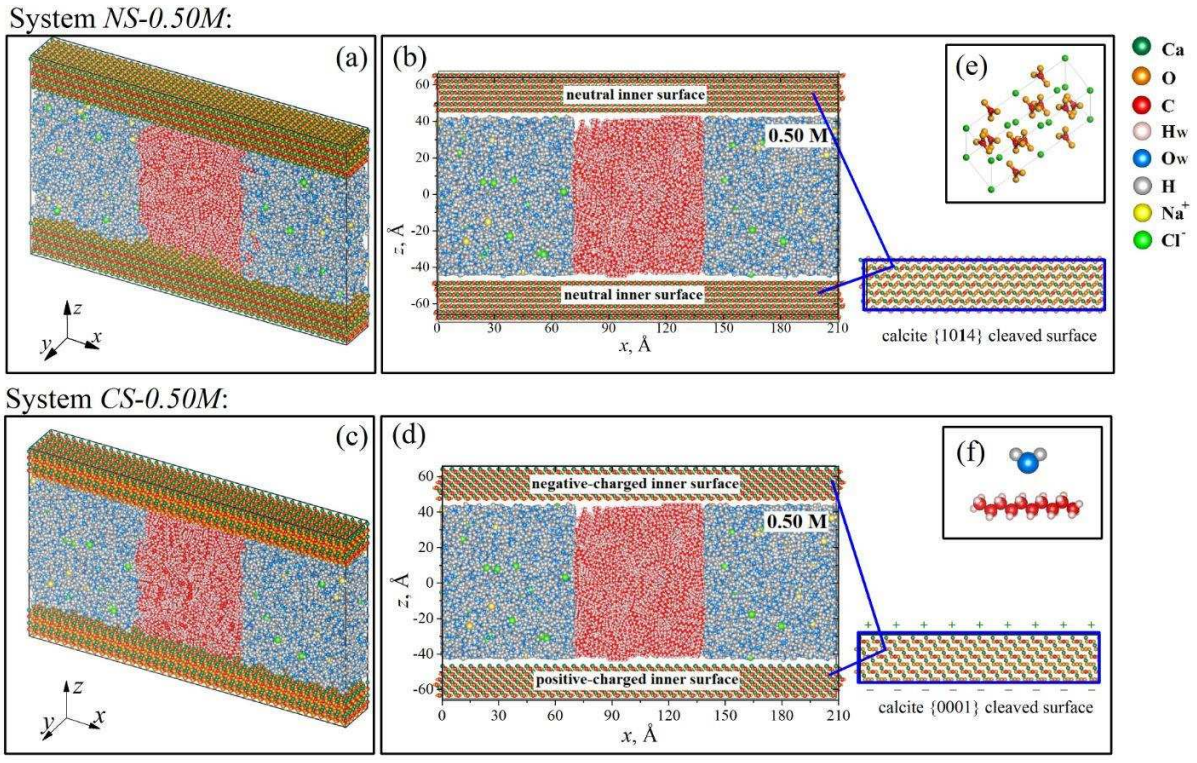

Fig. 1. Schematic illustration of initial configurations: (a) Perspective view of System "NS-0.50M", (b) Side view of System "NS-0.50M", with zoom-in image of calcite $\{10\bar{1}4\}$ surface, (c) Perspective view of

System “CS-0.50M”, (d) Side view of System “CS-0.50M” with zoom-in image of calcite {0001} surface, (e) The unit cell of calcite, $CaCO_3$, (f) Atomistic structure of water (H_2O) and n-decane ($C_{10}H_{22}$)

The walls of the slit nano-pore were composed of two parallel calcite surfaces, where the length along the x-axis direction and the separation distance between the mineral surfaces along the z-axis direction were fixed at 21 nm and 9 nm, respectively. The rhombohedral structure of calcite, which has space group $R\bar{3}c$, and hexagonal unit cell parameters a = b = 4.988 Å, c = 17.061 Å; $\alpha = \beta = 90°$, $\gamma = 120°$ [42] was used to create an atomistic model of the calcite surfaces. Calcite $\{10\bar{1}4\}$ and {0001} cleavage surfaces [43-45] were considered as representative of neutral and charged slabs to form nano-slit walls. In the case of calcite $\{10\bar{1}4\}$ surfaces, Ca^{2+} and CO_3^{2-} are located in the same layers, and this close packed and alternating arrangement of the oppositely charged ions makes the calcite $\{10\bar{1}4\}$ surface overall non-polar and neutral. Concerning the {0001} form of calcite, it contains alternating planes of Ca^{2+} and CO_3^{2-} groups situated in separate layers, as a result that the calcite {0001} plane is terminated by either Ca^{2+}-rich (carrying positive charge) or CO_3^{2-} rich (carrying negative charge), leading to a positively or negatively charged surface, respectively. Here, each calcite slab contains six and seven atomic layers (perpendicular to the x direction) for the calcite $\{10\bar{1}4\}$ and {0001} surface, which is sufficient to reproduce bulk-like properties at the centre of the slab and to obtain a careful description of the surface [46-48].

For the fluid in the pore region between the two mineral slabs, two rectangular aqueous electrolyte blocks were built with a 7-nm separation distance along the x-axis direction, and the intervening volume element was filled with oil molecules initially randomly orientated. As a simulant for the hydrocarbon-bearing geofluids, neutral non-polar n-decane ($C_{10}H_{22}$) was used as the representative non-polar oil phase. Decane is a typical component of petroleum and has been

presented frequently in the literature as a kerosene surrogate or as the main component of diesel surrogates. Aqueous sodium chloride (NaCl) solution was employed as the salt water phase to simulate geological fluids (brines). The number of water and decane molecules was calculated using a water density of 0.998 g/cm^3 and oil density of 0.730 g/cm^3, respectively. All the ions were initially randomly inserted into the aqueous region to avoid biased adsorption. Water salinities of 0.20 M, 0.50 M, and 1.00 M were applied to investigate the effect of salt concentration on the wettability of each mineral surface.

In total, six separate initial configurations were set up for both EMD and NEMD simulations with the variations of surface charge and water salinity, namely, NS-0.20M, NS-0.50M, NS-1.00M, CS-0.20M, CS-0.50M and CS-1.00M, respectively (where "NS" and "CS" stand for Neutral Surface and Charged Surface respectively; followed by a number as a specification of the water salinity in Molarity unit "M"). All configuration snapshots were rendered using the VESTA software [49]. It is notable that, for each simulation, the parallel calcite slabs were fixed, and two gaps of 5 Å were introduced to the top and bottom of the fluid simulation cell to avoid any unphysical interactions amongst fluid species at the mineral surfaces.

2.2 Force Fields Employed in the Simulations

The Simple Point Charge / Extended (SPC/E) rigid water model [50] was used to describe water molecular-interactions. The OPLS-AA (Optimized Potentials for Liquid Simulations – All Atoms) force field [51] was utilized to describe the interactions among atoms in the n-decane phase. This force field is parameterized for organic systems and has been demonstrated to reproduce physically accurate representations of hydrocarbons and similar organic molecules, and is compatible with SPC/E water [52]. The ions were modelled as charged

Lennard-Jones particles, with potential parameters proposed by Koneshan et al. [53]. The model developed by Raiteri et al. [48] was employed to model calcite surfaces. This model has been shown to be consistent with the other force fields applied [54]. Full details about the force field parameters employed are listed in Table S1 and Table S2 (in the Supplementary Material). The total energy is given by Equation 1, including both the intra- and intermolecular interactions:

$$E_{total} = E_{bond} + E_{angle} + E_{dihedral} + E_{torsion} + E_{vdw} + E_{coulombic} \quad (1)$$

where E_{total}, E_{bond}, E_{angle}, $E_{dihedral}$, $E_{torsion}$, E_{vdw} and $E_{coulombic}$ are the total energy, bond-stretching, angle-bending, dihedral-energy, torsion energy, van der Waals and electrostatic components, respectively. The Lennard-Jones potential parameters (ε_{ij} and σ_{ij}) between different atom types, were obtained using geometric combining rules as shown in Equations 2 and 3 [55]:

$$\sigma_{ij} = \sqrt{\sigma_{ii}\sigma_{jj}} \quad (2)$$

$$\varepsilon_{ij} = \sqrt{\varepsilon_{ii}\varepsilon_{jj}} \quad (3)$$

2.3 Equilibrium Molecular Dynamics Simulation (EMD)

All EMD calculations were performed using the DL_POLY simulation package [56]. The equations of motion were solved by the leap-frog algorithm with a SHAKE subroutine with a time step of 0.5 fs. The potential energy was evaluated with a 12.0 Å cut-off for the short-range van der Waals interaction, and the Ewald summation method for the Coulombic interactions (Smoothed Particle Mesh Ewald in DL_POLY) was calculated with a precision of 1×10^{-6}. Every simulation was initialized with an energy minimization run to reduce excessive forces for the system. The minimization procedure was accomplished using the steepest descents algorithm. Subsequently, all the simulations were run for a 50 ps equilibration period in a constant number

of particles, pressure and temperature (NPT) ensemble with a velocity-rescale Berendsen thermostat. This equilibration period was followed by a 5 ns production run in the NVT ensemble where the number of particles (N), the simulation box volume (V), and the temperature (T) were kept constant. The periodic boundary conditions were applied to all three spatial dimensions. All simulations were run to present ambient conditions, a pressure of 1 bar, and a temperature of 300 K using a velocity scaling method. In geological environment, the fluid confined in nanopores is generally at conditions with relative high temperature and pressure. But it was still necessary to run the simulations at ambient rather than reservoir temperatures due to the limitation of the available calcite force field, which has been parameterized to model systems under ambient conditions. There is still no suitable potential available under reservoir conditions, and considerable validation would be required against, for example, neutron scattering data to ensure the force field holds for higher temperatures and pressures.

2.4 Non-Equilibrium Molecular Dynamics Simulation (NEMD)

All NEMD simulations were performed using the DL_POLY package [56] as well. The hydrodynamic behaviour of various water/n-decane/salts fluids confined in a slit pore constructed by calcite $\{10\bar{1}4\}$ and {0001} slabs was investigated. The specific strategy was started from the final equilibrium configurations calculated through EMD simulation, and then a constant external force F_x of 0.001 kcal/(mol·Å) was applied to each atom of the pore fluid. This large pressure gradient is necessary because the fluid flow through pores is slow, and it will take an extremely long simulation to achieve a stable flooding state. A further 4 ns NVT ensemble NEMD simulation was carried out for each system. The x-directional velocity of each water molecule confined in the slot pore region during the final 1 ns was sampled every 0.5 ps in bins

of width 0.20 Å in the z-direction and then averaged. The velocity of the n-decane molecular cluster was averaged for the final 1.0 ns to represent the velocity of the decane cluster.

3. Results and Discussion

In this part, we discuss firstly in Section 3.1 the validity of the force fields and simulation strategy by EMD in a reference case NS-0.50M. The surface charge effect on the water/oil/mineral equilibrium interactions are studied under the same water salinity of 0.50 M. Then in Section 3.2, both the surface charge and the water salinity effects on the wettability alteration of calcite surfaces are reported, and Section 3.3 presents the NEMD results by applying an external force field to investigate the wettability effect on the oil transport properties mimicking a flooding process.

3.1 EMD simulation of the surface charge effects

The validation of our simulations is firstly demonstrated by a careful benchmarking of the approach on a reference model NS-0.50M, composed of neutral calcite $\{10\bar{1}4\}$ surfaces as nanoslit pore walls and n-decane/salt-water (0.50 M) fluids, as illustrated in Fig. 1(a, b). The calculated interaction energy, temperature and pressure profiles presented in Fig. 2(a, b) were considered to be equilibrated after 5 ns of simulation time, which was confirmed by extending the simulation time by a further 3 ns (a total of 8 ns) with no significant changes observed in the relevant parameter values. This demonstrates that the simulation is sufficiently long for studying a realistic interface between two bulk phases. In addition, the radial distribution functions (RDF) of water and n-decane molecules were sampled as shown in Fig. 2(c, d).

The RDFs between water molecules shown in Fig. 2(c) show that g(r) equals zero at short distances as expected, which indicates strong repulsive forces between two water molecules in the short range. For the interactions between oxygen atoms the first peak occurs at 2.8 Å with g(r) reaching a value of 3, indicating that it is three times more likely to find two oxygen atoms in different water molecules at this separation. A slight secondary maximum, consistent with a second coordination sphere, is observed however at longer distances, g(r) between two water molecules approaches a value of one as expected, indicating there is no long-range order.

The interaction between two n-decane molecules can be seen from the RDF profile in Fig. 2(d). The RDF profile for n-decane molecules shown in Figure 2(d) has the similar shape as the distribution result by Ryckaert et al. [58], which has been abundantly adopted to be compared by previous researchers for identifying their n-alkane simulation results [59-63]. As far as the intermolecular correlations are concerned, it is clear that the oscillations around g(r) = 1 are close to the cut-off radius. Trans (T) and Gauche (G) conformation positions of carbon atom neighbours in a molecule can also be observed, followed with successive GT and TT conformations as marked in Fig. 2(d). To characterize the conformations of the n-decane molecules in the n-decane/vapour interface system, the probability density function (PDF) distribution for the n-decane molecules as a function of the internal dihedral angle $\Phi_{C\text{-}C\text{-}C\text{-}C}$ is also shown in Fig. 2(d), where the peaks observed at $\Phi_{C\text{-}C\text{-}C\text{-}C} = 0°$ and $\Phi_{C\text{-}C\text{-}C\text{-}C} = \pm 120°$ correspond respectively to trans (T) and gauche (G^+ and G^-) conformations. The magnitudes of the G^+ and G^- peaks are very close, corresponding to the symmetry of the dihedral potential energy. The RDF profiles of both n-decane and water components are in good agreement with previous MD simulations and experimental results with no shifts for the two main peaks [57, 58]. To further validate our system setup and the applied force field, more MD simulations for

water/n-decane/vacuum equilibrium interactions have already been conducted and compared our calculated physical properties, i.e. interfacial tensions, contact angles, etc., with available experimental and simulation results [64].

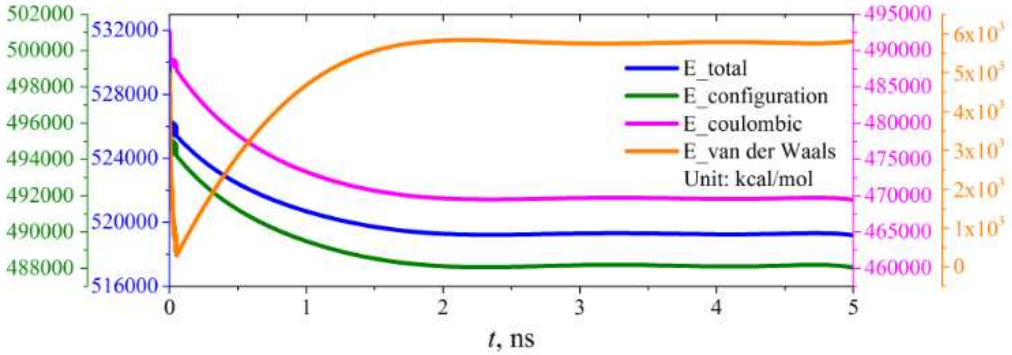

(a) Interaction energy profiles

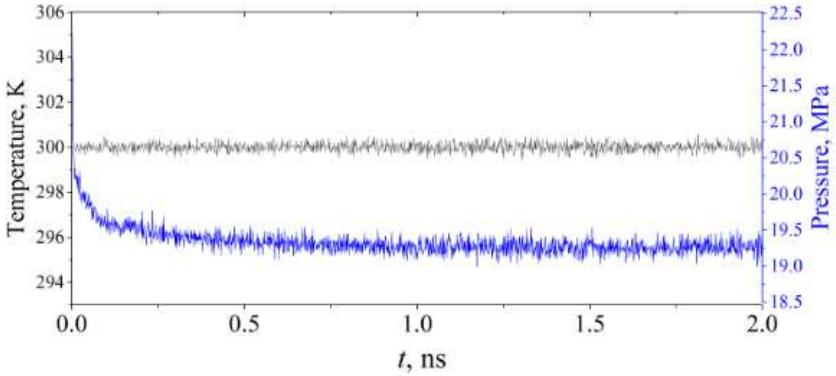

(b) Pressure and temperature profiles

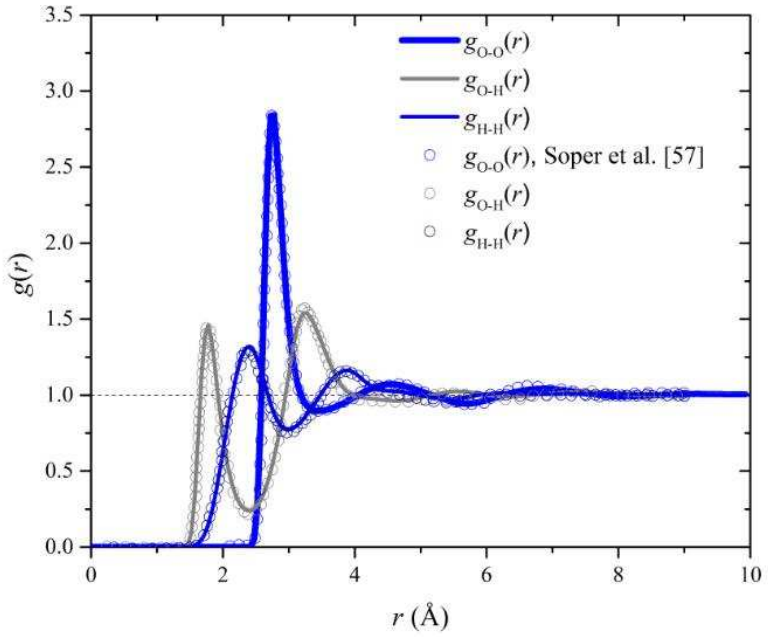

(c) RDF for water molecules

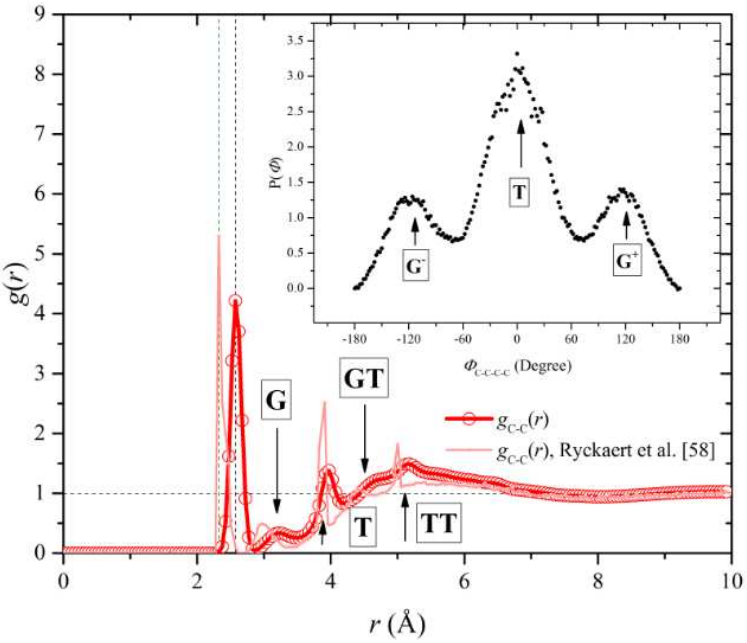

(d) RDF for n-decane molecules

Fig. 2. Illustration of (a) interaction energy, pressure and (b) temperature profiles during the equilibrium process, and RDF profile validations [57, 58] of (c) water and (d) n-decane phase in NS-0.50M system

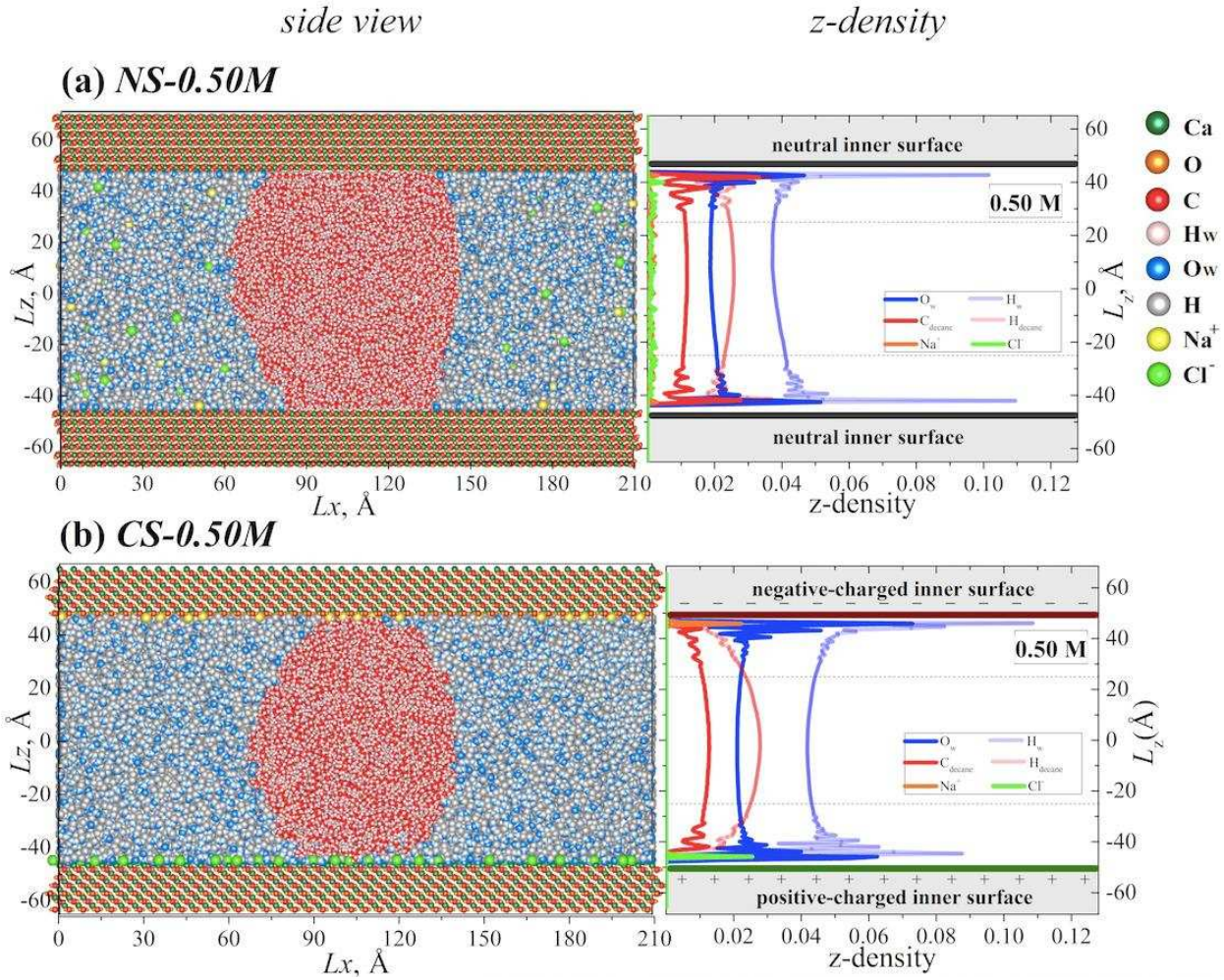
side view
z-density
(a) NS-0.50M
neutral inner surface
0.50 M
neutral inner surface
Lz, Å
Lx, Å
z-density
Lz (Å)
Ca
O
C
Hw
Ow
H
Na+
Cl-
(b) CS-0.50M
negative-charged inner surface
0.50 M
positive-charged inner surface
Lz, Å
Lx, Å
z-density
Lz (Å)

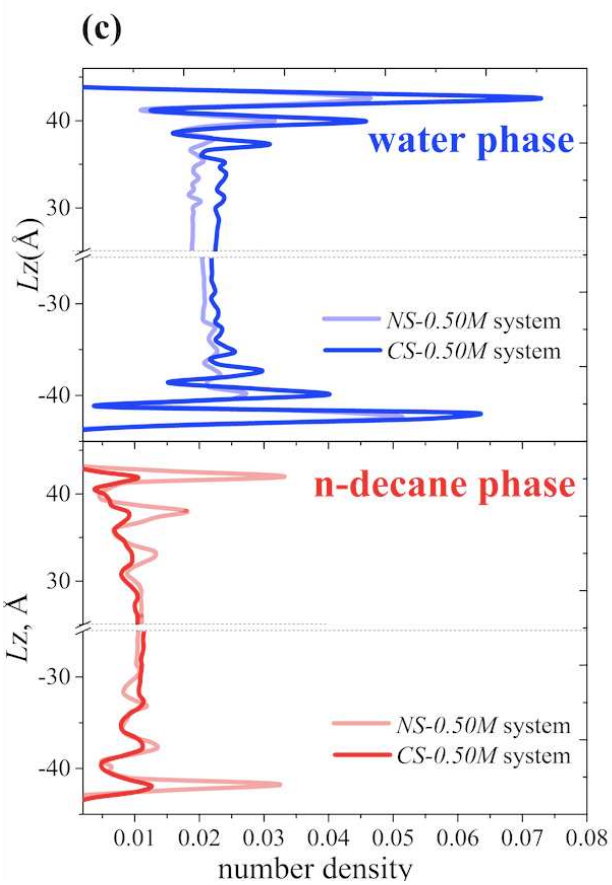

Fig. 3. Side view snapshots of final equilibrium configuration and corresponding number density profiles along z-axis direction for (a) NS-0.50M and (b) CS-0.50M systems, with (c) zoom-in comparison profiles of water and n-decane phase distributions near the calcite pore surfaces

To investigate the surface charge effect on the water/oil/mineral equilibrium interactions, the final-configuration snapshots of the salt-water/n-decane/calcite systems with neutral and charged pore wall surfaces (systems NS-0.50M and CS-0.50M) after 5 ns EMD simulation period are presented in Fig. 3, along with the corresponding number density profiles of each species in the z-axis direction. The results show that n-decane phases for both systems are aggregated and formed as droplet-like clusters, surrounded by the salt water phase. Na^+ and Cl^- ions in both systems are found to always remain in the water phase, without any diffusion into the oil phase. The water and n-decane phases are immiscible, forming a curved interface due to the interfacial tension effect. However, different n-decane wettability on the mineral pore walls can be found

from the different adsorbing state of n-decane clusters caused by the pore surface charge. For the system NS-0.50M with the neutral pore surfaces, the solid slabs exhibit partial decane-wettability, with parts of the n-decane molecules directly adsorbing onto the surface, as shown in Fig. 3(a); In contract, for system CS-0.50M with the charged pore surface, both positive-charged and negative-charged slabs ({0001} Ca^{2+} and {0001} CO_3^{2-} surfaces) manifest greater hydrophilic characteristics.

The atomic number density distributions along the z-axis direction for both systems in Fig. 3 are obtained by averaging the trajectories of each atomic species along the last 1 ns of the equilibrium simulations. The water and n-decane phase z-density profiles close to the pore wall region, as enlarged in Fig. 3(c), show that the confining of the surface causes both water and n-decane molecules to adopt particular configurations near the calcite surfaces, forming structured adsorption layers. Such an observation is consistent with the experimental results of Geissbuhler et al [65] via the surface X-ray scattering method, and the MD simulation results of Kerisit et al [66]. For system NS-0.50M, the appearance of the first n-decane peak in Fig. 3(c) shows that the neutral calcite surface is partially oil-wet. This is consistent with the direct visualization from the configuration snapshots after equilibration. For system CS-0.50M with charged surfaces, the reduced peak of the n-decane phase near the surface in the z-density profile indicates that both the upper and lower mineral surfaces ({0001} Ca and {0001} CO_3 surfaces) become more hydrophilic.

The distinctive difference in the distribution of ions between the cases of charged and non-charged surfaces can be visualized in Fig. 4(a). Instead of randomly distributing in the water phase as for the neutral system NS-0.50M, Na^+ and Cl^- ions in system CS-0.50M are adsorbed by the {0001} CO_3^{2-} and {0001} Ca^{2+} surfaces respectively, which is driven by the strong

electrostatic interactions between ions and the charged surfaces: (1) At each layer of the {10$\bar{1}$4} surface, Ca^{2+} and CO_3^{2-} ions are arranged alternately, which consequently makes the direct coordination of the sodium or chloride ions to the neutral calcite surface unfavourable. (2) The {0001} surface contains alternating planes of Ca^{2+} and CO_3^{2-} ions, which produces a dipole moment perpendicular to the surface. Polar surfaces are unstable by themselves and need either reconstruction to neutralize the dipole moment or to adsorb ions to remove the dipole moment. The distribution of cations and anions is therefore influenced by both {0001} CO_3^{2-} termination and {0001} Ca^{2+} termination, respectively. After reaching equilibrium, Cl^- ions make direct contact with the Ca^{2+} atoms on the {0001} Ca^{2+} termination, which is consistent with MD results by Vasconcelos et al. [67]. Such distinct differences of the adsorption behaviour are originated from different electrostatic interactions between the ions and surfaces.

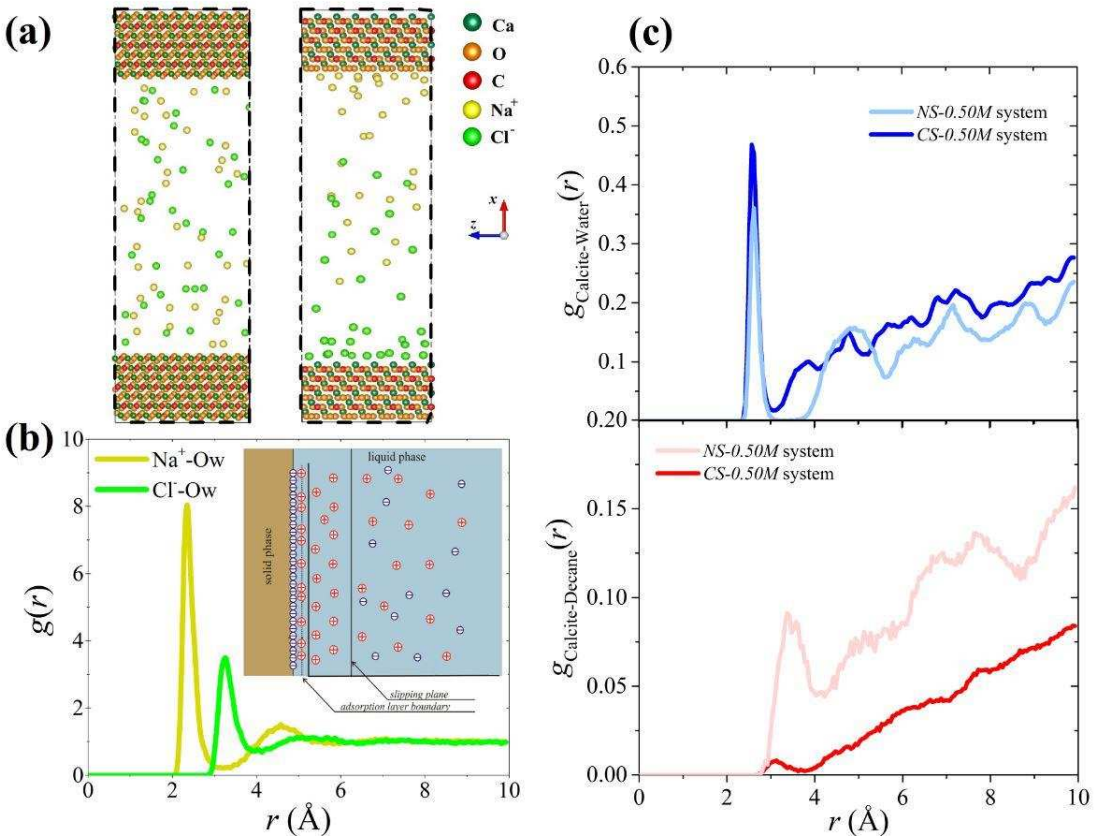

Fig. 4. Illustrations of (a) the ion distribution visualization in NS-0.50M and CS-0.50M systems, and the RDF profiles of system CS-0.50M for (b) ions/water, (c) water/calcite, and n-decane/calcite interactions

As reviewed earlier, several mechanisms have been proposed to explain the low-salinity effect for enhanced oil recovery, including electric double layer (EDL) expansion, multi-component ionic exchange and pH level reaction. The ion distributions following equilibration observed in this work suggests that EDL theory could explain the salinity effect for charged surfaces, where Na^+ and Cl^- ions exhibit an EDL distribution effect due to the opposite surface charge. The ions are predominantly fully coordinated by water molecules, which can be observed from the radial distribution functions (RDF or g(r)) profiles shown in Fig. 4(b). Both Na^+ and Cl^- have great hydration capacity and can induce water molecules close to the calcite surfaces, as reflected by the dominant peak appearing in Fig. 4(b). For instance, the sharp peaks indicate the highly ordered water structure around Na^+ ions, and the first valleys of the Na^+- O_w RDF are deep and wide indicating that the first and second solvation shells are clearly separated. The first maximum of the RDF is at 2.43 Å for Na^+, consistent with previous work [68]. Such a strong peak suggests that dense water clusters are formed around Na^+, which can diffuse with Na^+ in the solution. The RDF profile of salt water/decane/calcite interactions for both systems, Fig. 4(c), clearly shows that the surface charge has significant effects on both water/calcite interactions and decane/calcite interactions. The sharp peak in calcite/water RDF profile at 2.6 Å suggests that water is adsorbed on both neutral and charged surfaces, consistent with the MD results of Cooke et al. [69]. Both the reduced maximum-value in the dominant peak of the calcite/water RDF profile and increased maximum-value in the dominant peak of the calcite/n-decane RDF profile for CS-0.50M system in Fig. 4(c) suggest weaker n-decane molecule adsorptions on the charged surface. It can be concluded that charged pore surfaces combining with the effect of salinity can

lead to improved water-wet performance due to electrostatic interactions between the ions and surfaces, and the ion hydration effects.

3.2 EMD simulation of the surface charge and salinity effects

To reveal the effect of salinity and surface charge on the surface wettability, three salt water concentrations of 0.20 M, 0.50 M and 1.00 M were simulated along with two types of pore walls (i.e., neutral inner surface, and charged inner surface), which simulations are named as NS-0.20M, NS-0.50M, NS-1.00M, CS-0.20M, CS-0.50M, and CS-1.00M, respectively.

The final equilibrium configuration snapshots after 5 ns simulations are presented in Fig. 5, along with the z-density profiles for each species. Dominant peaks of the water phase, from z-density profiles, close to the solid-pore surfaces appear in all cases, which indicate the presence of structured layers of water due to water adsorption onto the pore walls. Away from the near pore-wall region, uniform bulk properties are observed for both water and n-decane phases. The salinity appears to have less effect on the water/n-decane wettability for the neutral pore, as shown in Fig. 5(a-c). Fig. 5(d-f) shows that the wettability alteration due to the charged calcite {0001} surface, in contrast, is highly dependent on the salinity of the confined fluid. At a salinity of 0.20 M with charged pore surfaces (system CS-0.20M), the {0001} surface exhibits partial decane-wettability, with decane molecules directly interacting with the surface. However, as the water salinity increase, the contact area between n-decane and the calcite surface decreases. At a salinity of 0.50 M (system CS-0.50M), both calcite {0001} Ca^{2+} and {0001} CO_3^{2-} surfaces manifest greater hydrophilic characteristics. With a further increase of water salinity in the CS-1.00M system, the calcite surface becomes completely water-wet.

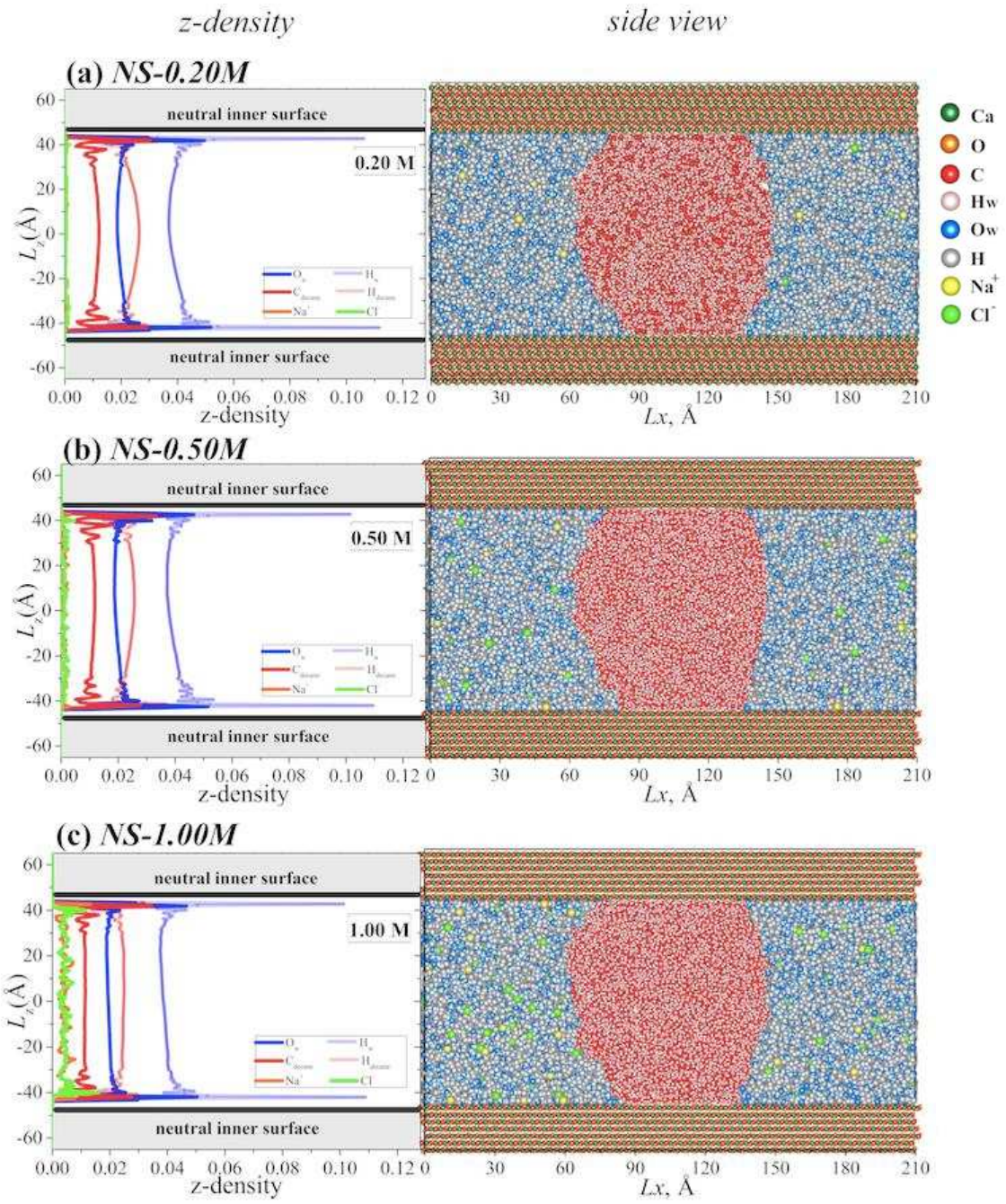
z-density
side view
(a) NS-0.20M
neutral inner surface
0.20 M
neutral inner surface
(b) NS-0.50M
neutral inner surface
0.50 M
neutral inner surface
(c) NS-1.00M
neutral inner surface
1.00 M
neutral inner surface
L_z (Å)
z-density
Lx, Å
Ca
O
C
Hw
Ow
H
Na^+
Cl^-

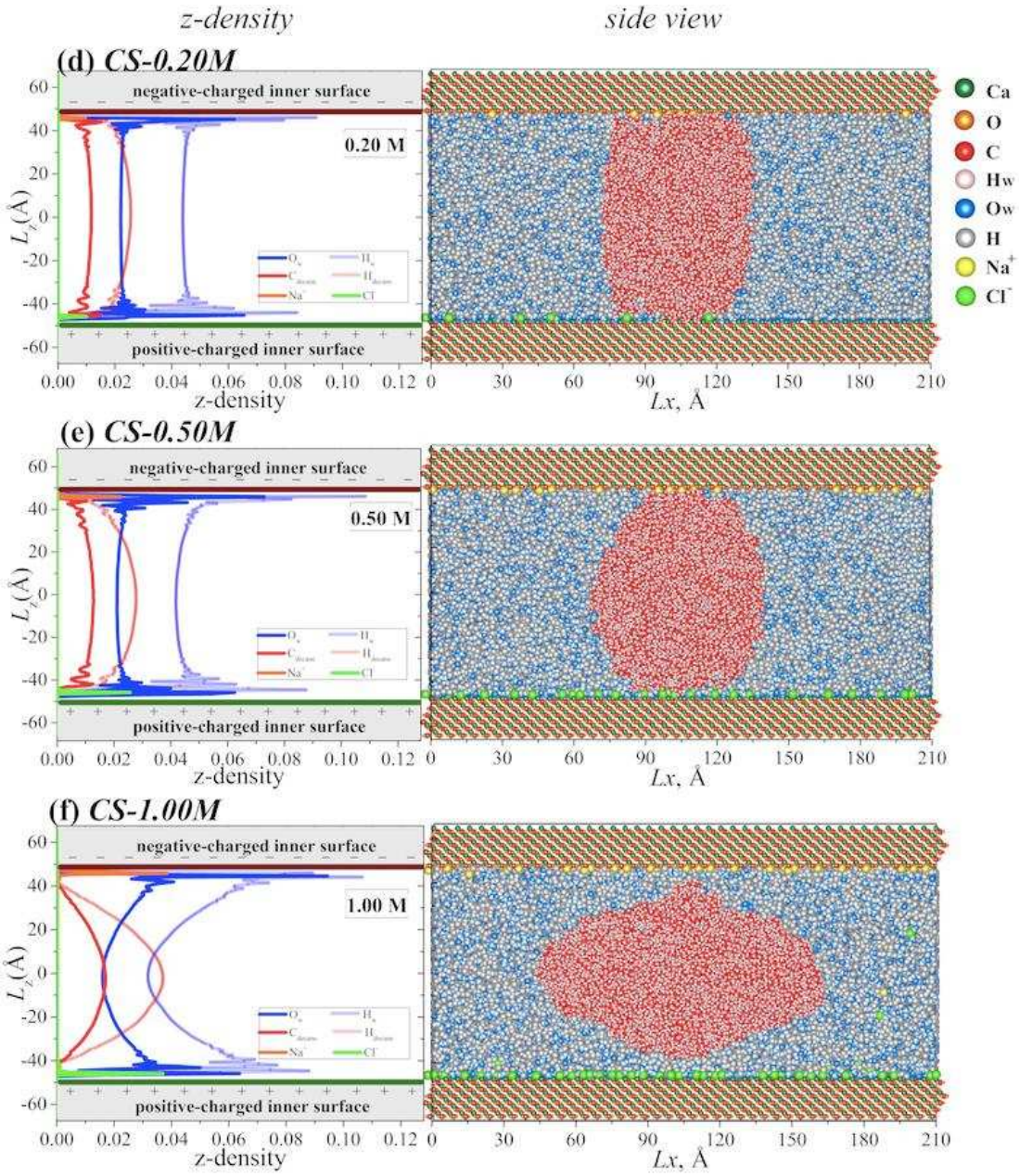
z-density
side view
(d) CS-0.20M
negative-charged inner surface
0.20 M
positive-charged inner surface
z-density
Lx, Å
(e) CS-0.50M
negative-charged inner surface
0.50 M
positive-charged inner surface
z-density
Lx, Å
(f) CS-1.00M
negative-charged inner surface
1.00 M
positive-charged inner surface
z-density
Lx, Å
Ca
O
C
Hw
Ow
H
Na+
Cl-

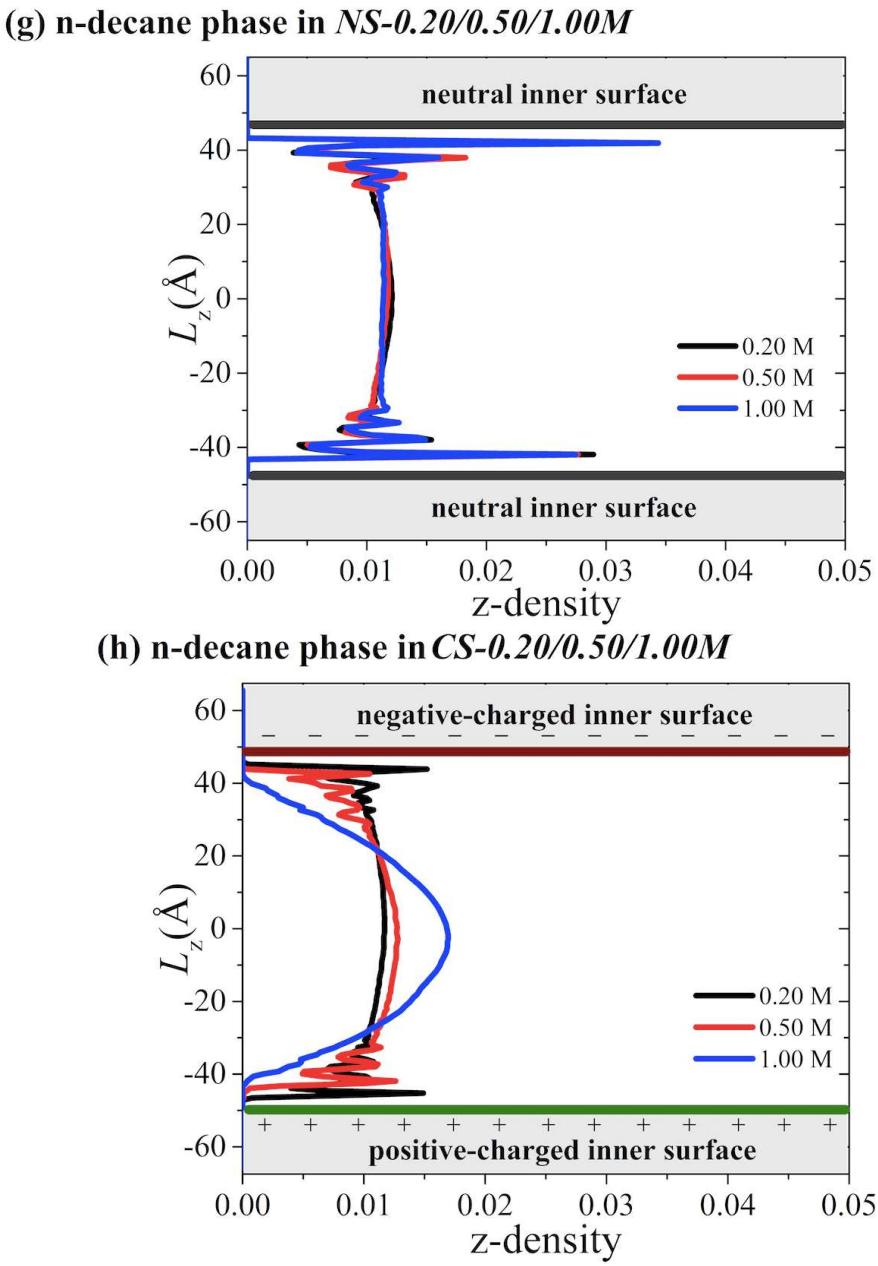

Fig. 5. Combination effects of the pore surface charge and water salinity on the oil adsorption in a nano pore: (a-f) number density profile along z-axis direction, and corresponding xz-plane side view snapshot of final equilibrium configuration for each system, (g) n-decane phase number density along z-axis direction with variations of water salinity in a neutral pore, (h) n-decane phase number density along z-axis direction with variations of water salinity in a charged pore

Comparisons of salinity effect on the n-decane phase distribution along the z-axis direction are presented in Fig. 5(g, h). Fig. 5(g) shows that the water salinity has little effect on the n-decane molecular distribution for neutral surfaces. However, for nano-pores with charged inner surfaces, the maximum value of the dominant peak of the n-decane phase close to the

fluid/wall interfaces decreases when the salinity is increased from 0.20 M to 0.50 M. At a water salinity of 1.00 M, no adsorption of n-decane molecules on the charged pore wall is observed with the total disappearance of the peaks close to the near-wall regions, as shown in Fig. 5(h).

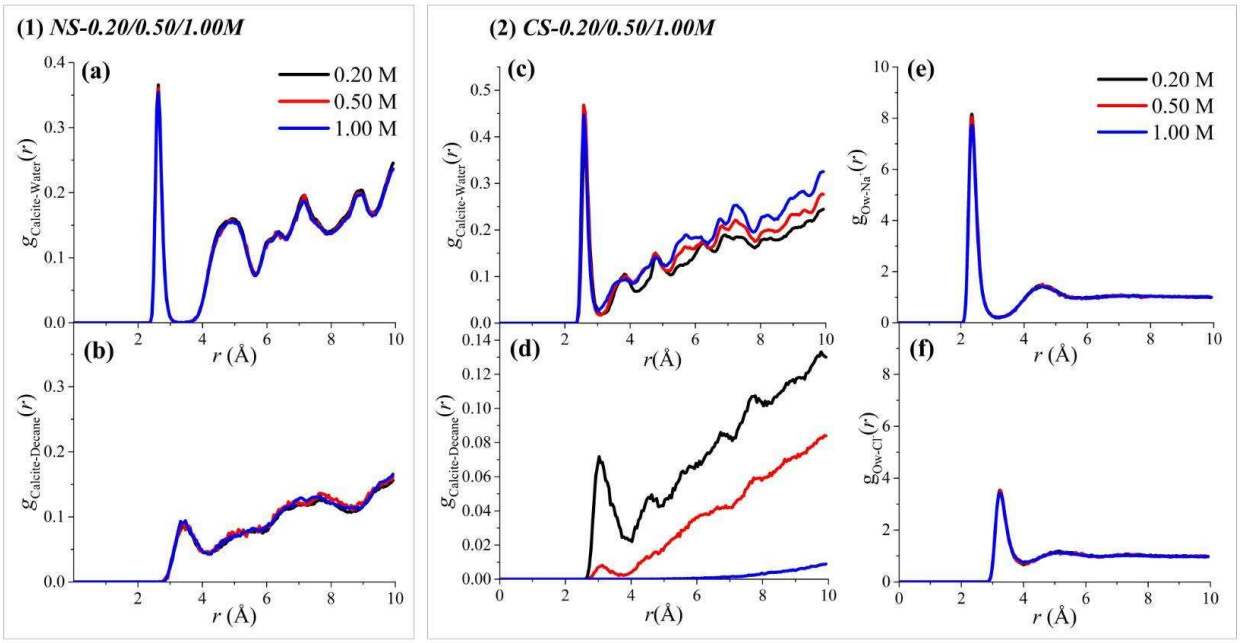

Fig. 6. Radial distribution function profiles for (1) NS-0.20M/0.50M/1.00M systems and (2) CS-0.20M/0.50M/1.00M systems

RDF profiles from Fig. 6(a, b), demonstrate the water/calcite and n-decane/calcite interactions for systems with neutral pore surfaces. With an increase in water salinity from 0.00 M to 1.00 M, little effect can be observed on either the water/calcite or decane/calcite interactions. In contrast, RDFs for charged pore surfaces, as shown in Fig. 6(c, d), show that the hydrophilicity of charged calcite surfaces can be enhanced by increasing the salt concentration. For n-decane/calcite interactions, as shown in Fig. 6(d), the maximum values of the first peaks, at around 3.2 Å, gradually decrease with the decrease in salinity. At 1.00 M, the peak vanishes indicating a completely water-wet condition.

RDF profiles for sodium and chloride ions interacting with water molecules for CS-0.20M/0.50M/1.00M systems are illustrated in Fig. 6(e, f). It is observed that an increase in water salinity has less impact on the hydration effect of ions in the aqueous solution. However, for the systems with charged pores, the increase in water salinity leads to an increase in counter-ions, which results in an enhancement of surface hydrophilicity. Previous MD simulations of charged clay-layers also indicated the influence of counter-ions on the wettability of charged surfaces [33, 36, 40], consistent with our simulation results, revealing that the hydrophobicity of charged calcite surface decreases with an increase in water salinity. Taking experimental work [40, 70] as an example, incorporation of Li^+ into the carbonate layer could result in preferential stabilization of the {0001} calcite surfaces by the neutralization of the surface dipole without the requirement for surface reconstruction. Thus, the growth is relatively fast with the consequence that the {0001} face is not observed under normal, synthetic conditions through experimental approaches. The relatively high Li^+ concentrations required in the above experiments suggests a specific electrostatic shielding of the {0001} face due to Li^+ ions located in surface sites.

It can be concluded that with the increase of water salinity, strong electrostatic interactions between ions and charged surface can be found, which can cause strong ion adsorption at a distance away from the inner sphere complexes to cause the EDL expansion effect. The strong hydration effects of the adsorbed ions on the charged surface can promote surface wettability towards increased hydrophilicity which is beneficial for oil detachment.

3.3 NEMD simulation of the wettability effect on the oil transport

Using NEMD simulation methods, the effect of surface wettability on the hydrodynamics of pore fluids during the flooding process is reported in this section for EOR applications. All NEMD calculations were conducted by resuming simulations from the final configuration

computed from the previous 5 ns EMD simulations whilst applying a constant external force F_x of 0.001 kcal/(mol·Å) to the pore fluid.

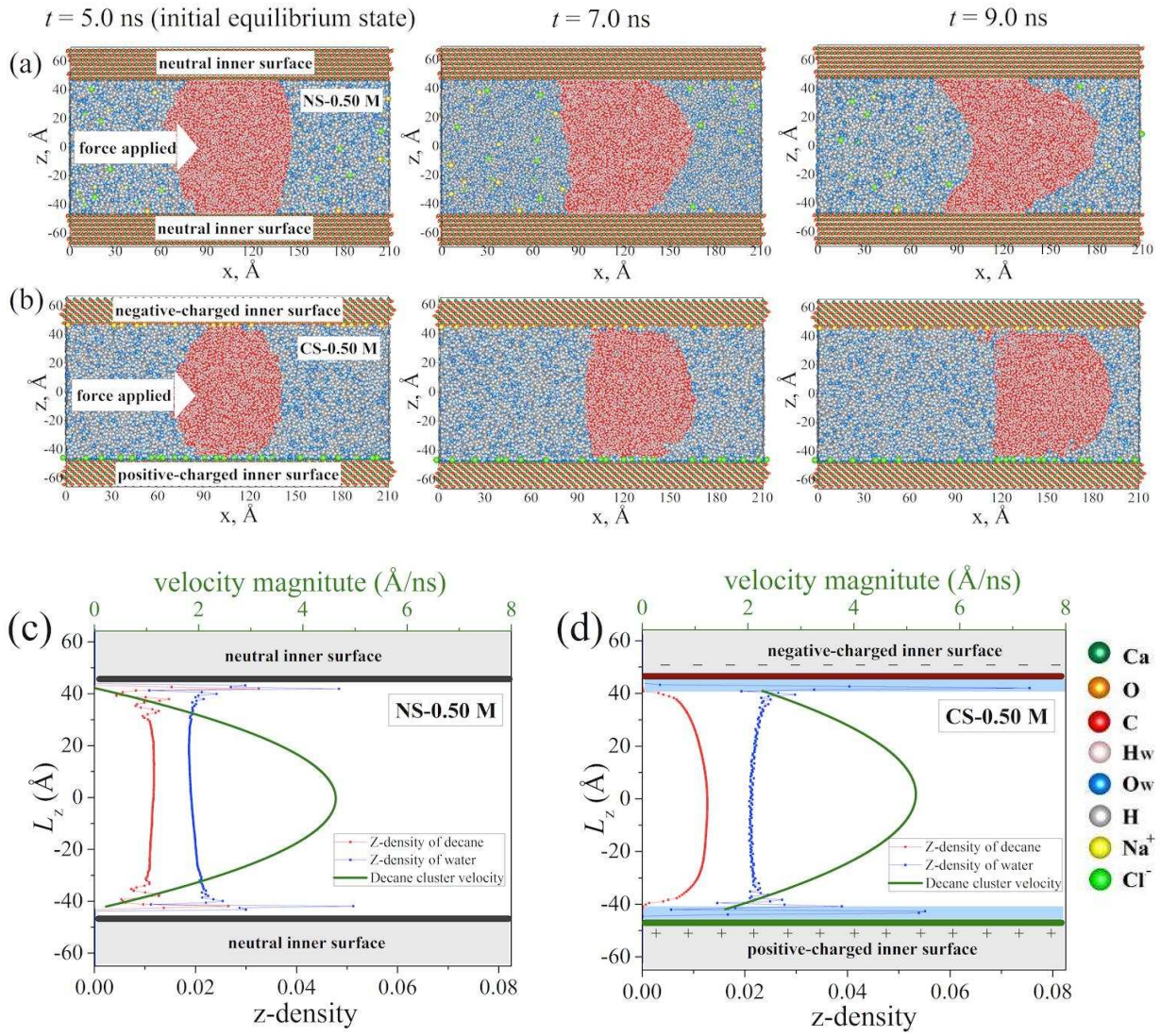

Fig. 7. The configuration snapshots during the NEMD simulations for (a) *NS-0.50M* system and (b) *CS-0.50M* system, associating with the average z-density profiles of each phases, and the average n-decane velocity profile along z-aixs directions for (c) *NS-0.50M* system and (d) *CS-0.50M* system

As illustrated in Fig. 7(a), the NEMD simulation for system NS-0.50M starts from the equilibrium wettability state after 5 ns, where the neutral calcite surface is, initially, partially hydrophobic through oil adsorption. By introducing an external force F_x, the fluids confined in the nano slit pore are displaced as the flooding proceeds. The multiphase fluid-distribution

configuration snapshots after another 4 ns show that all n-decane molecules move as a cluster under the external force. Due to the partial oil-wettability, the velocity of the oil interface near to the calcite slab boundary is much slower than that of the middle bulk-phase, as shown in Fig. 7(c), which leads to the formation of a meniscus interface during the flooding process. The oil adsorption effects can also be observed from the dominant peak of the decane z-density profile, shown in Fig. 7(c). This phenomenon indicates that oil adsorption can restrict the mobility of the oil interface close to the calcite slabs with lower velocities in the pore boundary region, which is disadvantageous for EOR applications.

Compared with the neutral system, the initial equilibrium configuration for the CS-0.50M system exhibits more water-wet characteristic, as shown in Fig. 7(b), due to the effects of ions and surface charge on the wettability. When fluid is displaced under this water-wet condition, the movement of decane molecules is quite distinct from that in system NS-0.50M. The velocity of the n-decane cluster close to the pore surface is much greater, as presented in Fig. 7(d). This phenomenon can be attributed to the effects of wettability alteration, which convert the slab inner-boundary into a hydrophilic surface as shown by the dominant peak of water z-density profile near the slabs in Fig. 7(d). The n-decane cluster is hence expelled from the slit pore walls by a shielding layer of water molecules. Overall, n-decane molecules tend to migrate faster than with the non-charged surface, showing the significant influence of the hydrophilicity of the wall.

As shown in Fig. 8(b), with a further increase in the salt concentration to 1.00 M, compared with system CS-0.50M, the hydrophilicity of pore walls in system CS-1.00M is enhanced due to stronger ion hydration effects. n-Decane molecules tend to aggregate together and are completely detached from the charged surface, transporting collectively as a cluster under the external force. Both the water/decane z-density profiles and velocity profile of the

decane cluster are apparently unsymmetrical in Fig. 8(d), corresponding to the different hydration intensities of sodium and chloride ions, as shown in Fig. 4(b).

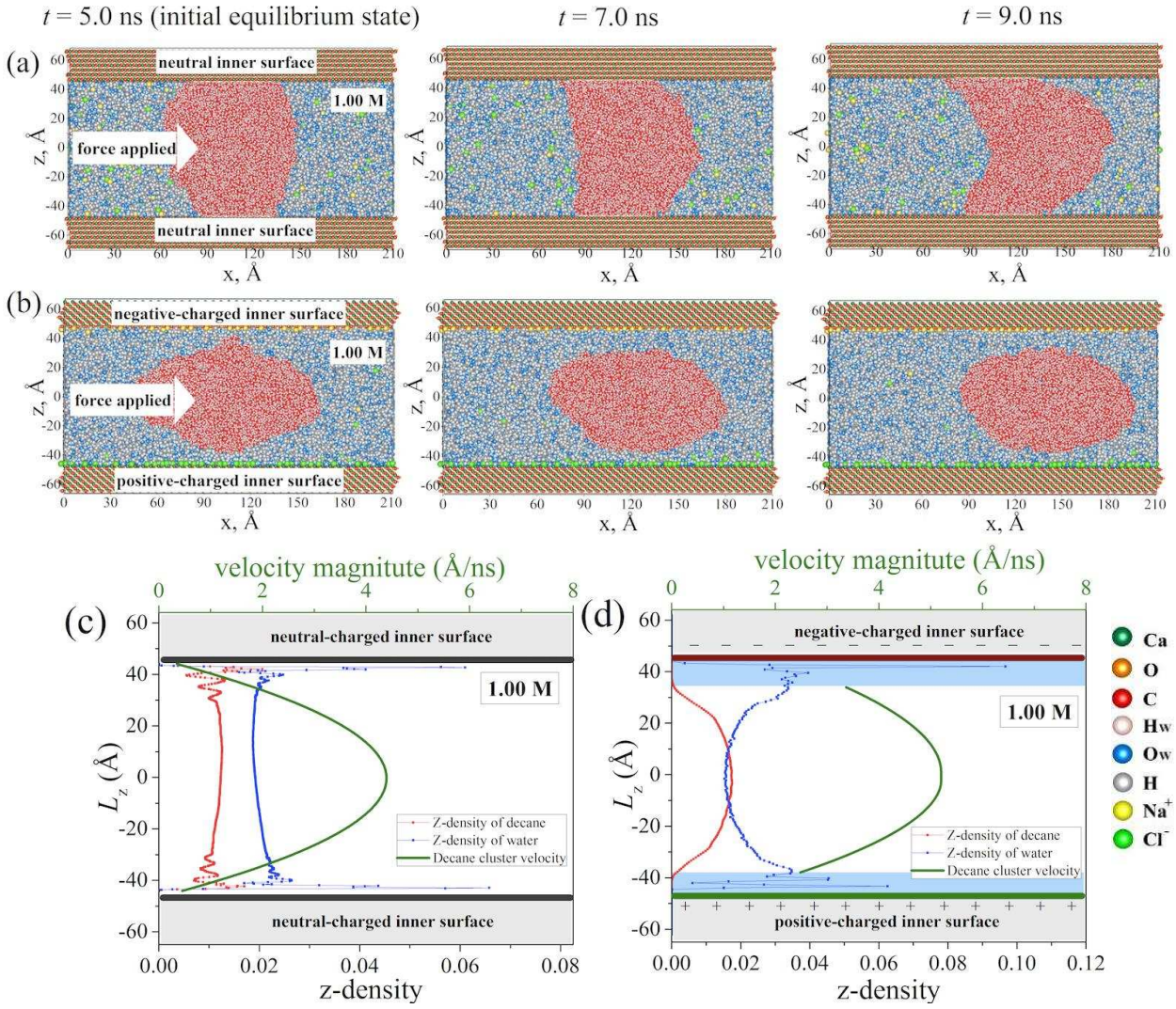

Fig. 8. The configuration snapshots during the NEMD simulations for (a) *NS-1.00M* system and (b) *CS-1.00M* system, associating with the average z-density profiles of each phases, and the average n-decane velocity profile along z-aixs directions for (c) *NS-1.00M* system and (d) *CS-1.00M* system

The centre-of-mass (COM) trajectories of the n-decane molecule-cluster in the xz plane, under different surface charge and water salinity conditions, are plotted in Fig. 9(a) to investigate the oil motion during the flooding process. The corresponding average velocity of n-decane along the x-axis direction is presented in Fig. 9(b). The analysis shows that better displacement performance can be obtained under conditions of greater water salinity in charged calcite nano-

pores, which is beneficial for enhanced oil recovery. Clearly the presence of hydrophilic surfaces in pore walls can greatly influence the hydrodynamics of the pore fluid.

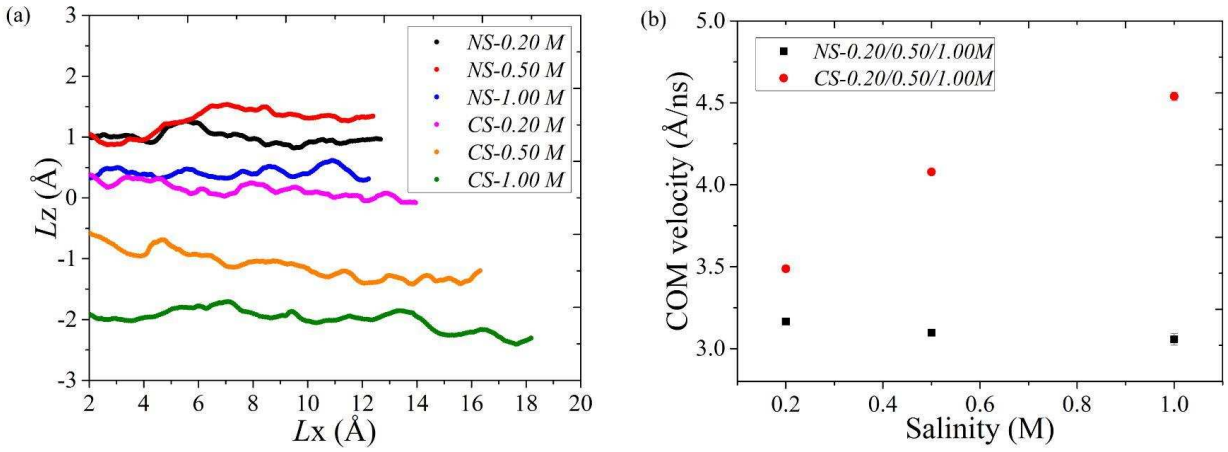

Fig. 9. n-Decane phase transport properties in a calcite nanopore: (a) Planar COM trajectories of the n-decane cluster, and (b) average velocity along the x-axis direction for all systems

4. Conclusions

The simulations presented address the effects of pore surface charge and water salinity on water/oil/minerals interactions (EMD), and oil displacement in a calcite nano-pore (NEMD). The results have been analysed in the context of addressing the mechanism underpinning the alteration of surface wettability in carbonate rock reservoirs. The simulation results can be summarized as followed:

(1) At a water salinity of 0.50 M, the nonpolar calcite nano-pore exhibits partially oil wet characteristics after equilibration with oil attaching and adsorbing onto the neutral surface. The charged calcite slit-pore caused a distribution of anion and cation through adsorption, in response to the electrostatic field, which altered the surface wettability to produce hydrophilic surfaces due to the hydration effect around the ions.

(2) An increase in water salinity did not affect significantly the oil wettability of the neutral calcite surface, and a random distribution of ions was maintained in the water phase. However,

for certain nano-slit pores with the natural occurrence of dipole layers, greater water salinity enhanced the mineral surface hydrophilicity by altering the surface from partially water wet to completely water wet due to the dipole – ion interactions. At a water salinity of 1.00 M, all n-decane molecules were completely detached from the charged mineral surface by the salt water shield layers.

(3) The non-equilibrium MD simulation results for the flooding process show that n-decane molecules tended to aggregate and transport as a cluster under the external flooding force. However, partial decane-wettability of calcite surfaces inhibited significantly the oil movement in the pore region. The combination of the effects of ion hydration and the electrostatic effect of ion adsorption on the dipolar nano-pore surfaces led to a clear enhancement in oil transport, and hence indicated the potential for increased oil recovery.

Acknowledgements

The authors appreciate financial support from a European Research Council Consolidator Grant (Grant Number: 648375) and the China Scholarship Council for a scholarship to support one of us, Jin Zhao, (No. 201506450021).

References

[1] Alvarado V, Manrique E. Enhanced oil recovery: an update review. Energies 2010;3(9):1529-1575.

[2] Morrow N, Buckley J. Improved oil recovery by low-salinity water flooding. J Petrol Technol 2011;63(05):106-112.

[3] Pereira JF, Costa R, Foios N, Coutinho JA. Ionic liquid enhanced oil recovery in sand-pack columns. Fuel 2014;134:196-200.

[4] Morrow NR. Wettability and its effect on oil recovery. J Petrol Technol 1990;42(12):1-476.

[5] Ershadi M, Alaei M, Rashidi A, Ramazani A, Khosravani S. Carbonate and sandstone reservoirs wettability improvement without using surfactants for Chemical Enhanced Oil Recovery (C-EOR). Fuel 2015;153:408-415.

[6] Tian H, Wang M. Electrokinetic mechanism of wettability alternation at oil-water-rock interface. Surf Sci Rep 2018.

[7] Myint PC, Firoozabadi A. Thin liquid films in improved oil recovery from low-salinity brine. Curr Opin Colloid Interface Sci 2015;20(2):105-114.

[8] Puntervold T, Strand S, Ellouz R, Austad T. Modified seawater as a smart EOR fluid in chalk. J Petrol Sci Eng 2015;133:440-443.

[9] Al Shalabi EW, Sepehrnoori K, Delshad M. Mechanisms behind low salinity water injection in carbonate reservoirs. Fuel 2014;121:11-19.

[10] Barnaji MJ, Pourafshary P, Rasaie MR. Visual investigation of the effects of clay minerals on enhancement of oil recovery by low salinity water flooding. Fuel 2016;184:826-835.

[11] Hilner E, Andersson MP, Hassenkam T, Matthiesen J, Salino PA, Stipp SL. The effect of ionic strength on oil adhesion in sandstone–the search for the low salinity mechanism. Sci Rep 2015;5:9933.

[12] McMillan MD, Rahnema H, Romiluy J, Kitty FJ. Effect of exposure time and crude oil composition on low-salinity water flooding. Fuel 2016;185:263-272.

[13] Nasralla RA, Nasr-El-Din HA. Double-layer expansion: is it a primary mechanism of improved oil recovery by low-salinity waterflooding?. SPE Reservoir Eval Eng 2014;17(01):49-59.

[14] Lashkarbolooki M, Riazi M, Ayatollahi S, Hezave AZ. Synergy effects of ions, resin, and asphaltene on interfacial tension of acidic crude oil and low–high salinity brines. Fuel 2016;165:75-85.

[15] Nasralla RA, Bataweel MA, Nasr-El-Din HA. Investigation of wettability alteration and oil-recovery improvement by low-salinity water in sandstone rock. J Can Petrol Technol 2013;52(02):144-154.

[16] Ghanbari E, Dehghanpour H. Impact of rock fabric on water imbibition and salt diffusion in gas shales. Int J Coal Geol 2015;138:55-67.

[17] Sheng JJ. Critical review of low-salinity waterflooding. J Pet Sci Eng 2014;120:216-224.

[18] Yousef AA, Al-Saleh SH, Al-Kaabi A, Al-Jawfi MS. Laboratory investigation of the impact of injection-water salinity and ionic content on oil recovery from carbonate reservoirs. SPE Reservoir Eval Eng 2011;14(05):578-593.

[19] Al-Anssari S, Barifcani A, Wang S, Maxim L, Iglauer S. Wettability alteration of oil-wet carbonate by silica nanofluid. J Colloid Interface Sci 2016;461:435-442.

[20] RezaeiDoust A, Puntervold T, Austad T. Chemical verification of the EOR mechanism by using low saline/smart water in sandstone. Energy Fuels 2011;25(5):2151-2162.

[21] Shariatpanahi SF, Hopkins P, Aksulu H, Strand S, Puntervold T, Austad T. Water based EOR by wettability alteration in dolomite. Energy Fuels 2016;30(1):180-187.

[22] Shariatpanahi SF, Strand S, Austad T. Evaluation of water-based enhanced oil recovery (EOR) by wettability alteration in a low-permeable fractured limestone oil reservoir. Energy Fuels 2010;24(11):5997-6008.

[23] Jackson MD, Al-Mahrouqi D, Vinogradov J. Zeta potential in oil-water-carbonate systems and its impact on oil recovery during controlled salinity water-flooding. Sci Rep 2016;6:37363.

[24] Austad T, Shariatpanahi SF, Strand S, Black CJ, Webb KJ. Conditions for a low-salinity enhanced oil recovery (EOR) effect in carbonate oil reservoirs. Energy Fuels 2011;26(1):569-575.

[25] Zhang P, Tweheyo MT, Austad T. Wettability alteration and improved oil recovery by spontaneous imbibition of seawater into chalk: Impact of the potential determining ions Ca^{2+}, Mg^{2+}, and SO_4^{2-}. Colloids Surf A 2007; 301(1): 199-208.

[26] Chen Y, Xie Q, Sari A, Brady PV, Saeedi A. Oil/water/rock wettability: Influencing factors and implications for low salinity water flooding in carbonate reservoirs. Fuel 2018;215:171-177.

[27] Mahani H, Keya AL, Berg S, Bartels WB, Nasralla R, Rossen WR. Insights into the mechanism of wettability alteration by low-salinity flooding (LSF) in carbonates. Energy Fuels 2015;29(3):1352-1367.

[28] Sakthivel S, Velusamy S, Nair VC, Sharma T, Sangwai JS. Interfacial tension of crude oil-water system with imidazolium and lactam-based ionic liquids and their evaluation for enhanced oil recovery under high saline environment. Fuel 2017;191:239-250.

[29] Kumar S, Mandal A. Studies on interfacial behavior and wettability change phenomena by ionic and nonionic surfactants in presence of alkalis and salt for enhanced oil recovery. Appl Surf Sci 2016;372:42-51.

[30] Wang FC, Wu HA. Enhanced oil droplet detachment from solid surfaces in charged nanoparticle suspensions. Soft Matter 2013; 9(33):7974-7980.

[31] Wang FC, Zhao YP. Contact angle hysteresis at the nanoscale: a molecular dynamics simulation study. Colloid Polym Sci 2013; 291(2):307-315.

[32] Li Y, Wu H, Wang F. Effect of a single nanoparticle on the contact line motion. Langmuir 2016;32(48):12676-12685.

[33] Underwood T, Erastova V, Cubillas P, Greenwell HC. Molecular dynamic simulations of montmorillonite–organic interactions under varying salinity: An insight into enhanced oil recovery. J Phys Chem C 2015;119(13):7282-7294.

[34] Underwood T, Erastova V, Greenwell HC. Wetting effects and molecular adsorption at hydrated kaolinite clay mineral surfaces. J Phys Chem C 2016;120(21):11433-11449.

[35] Underwood T, Greenwell HC. The Water-Alkane Interface at Various NaCl Salt Concentrations: A Molecular Dynamics Study of the Readily Available Force Fields. Sci Rep 2018;8(1):352.

[36] Zhang L, Lu X, Liu X, Yang K, Zhou H. Surface wettability of basal surfaces of clay minerals: insights from molecular dynamics simulation. Energy Fuels 2016;30(1):149-160.

[37] Khusainova A, Nielsen SM, Pedersen HH, Woodley JM, Shapiro A. Study of wettability of calcite surfaces using oil–brine–enzyme systems for enhanced oil recovery applications. J Pet Sci Eng 2015;127:53-64.

[38] Stipp SL, Konnerup-Madsen J, Franzreb K, Kulik A, Mathieu HJ. Spontaneous movement of ions through calcite at standard temperature and pressure. Nature 1998;396(6709):356-359.

[39] Ma YZ, Holditch S. Unconventional oil and gas resources handbook: Evaluation and development. Gulf Prof Publ 2015.

[40] Pastero L, Costa E, Bruno M, Rubbo M, Sgualdino G, Aquilano D. Morphology of calcite (CaCO3) crystals growing from aqueous solutions in the presence of Li^+ ions. Surface behavior of the {0001} form. Cryst Growth Des 2004;4(3):485-490.

[41] Material Studio Software. Accelrys Inc., San Diego, CA; 2010.

[42] Deer WA, Howie RA, Zussman J. An introduction to the rock-forming minerals. Hong Kong: Longman; 1992.

[43] Roberto MF, Marco B, Dino A. Effect of the Surface Relaxation on the Theoretical Equilibrium Shape of Calcite. 1. The [001] Zone. Cryst Growth Des 2010;10(9):4096-4100.

[44] Song RQ, Colfen H, Xu AW, Hartmann J, Antonietti M. Polyelectrolyte-directed nanoparticle aggregation: systematic morphogenesis of calcium carbonate by nonclassical crystallization. Acs Nano 2009;3(7):1966-1978.

[45] Shen JW, Li C, van der Vegt NF, Peter C. Understanding the control of mineralization by polyelectrolyte additives: simulation of preferential binding to calcite surfaces. J Phys Chem C 2013;117(13):6904-6913.

[46] de Leeuw N, Parker S. Atomistic simulation of the effect of molecular adsorption of water on the surface structure and energies of calcite surfaces. J Chem Soc Faraday Trans 1997;93(3):467-475.

[47] Raiteri P, Gale JD. Water is the key to nonclassical nucleation of amorphous calcium carbonate. J Am Chem Soc 2010;132(49):17623-17634.

[48] Raiteri P, Gale JD, Quigley D, Rodger PM. Derivation of an accurate force-field for simulating the growth of calcium carbonate from aqueous solution: A new model for the calcite− water interface. J Phys Chem C 2010;114(13):5997-6010.

[49] Momma K, Izumi F. VESTA: a three-dimensional visualization system for electronic and structural analysis. J Appl Crystallogr 2008;41(3):653-658.

[50] Berendsen HJ, Grigera JR, Straatsma TP. The missing term in effective pair potentials. J Phys Chem 1987;91(24):6269-6271.

[51] Jorgensen WL, Tirado-Rives J. The OPLS [optimized potentials for liquid simulations] potential functions for proteins, energy minimizations for crystals of cyclic peptides and crambin. J Am Chem Soc 1988;110(6):1657-1666.

[52] Ballal D, Venkataraman P, Fouad WA, Cox KR, Chapman WG. Isolating the non-polar contributions to the intermolecular potential for water-alkane interactions. J Chem Phys 2014;141(6):064905.

[53] Koneshan S, Rasaiah JC, Lynden-Bell RM, Lee SH. Solvent structure, dynamics, and ion mobility in aqueous solutions at 25 C. J Phys Chem B 1998;102(21):4193-4204.

[54] Fenter P, Kerisit S, Raiteri P, Gale JD. Is the calcite–water interface understood? Direct comparisons of molecular dynamics simulations with specular X-ray reflectivity data. J Phys Chem C 2013;117(10):5028-5042.

[55] Hansen JP, McDonald IR. Theory of simple liquids. Elsevier; 1990.

[56] Smith W, Yong CW, Rodger PM. DL_POLY: Application to molecular simulation. Mol Simul 2002;28(5):385-471.

[57] Soper AK. The radial distribution functions of water and ice from 220 to 673 K and at pressures up to 400 MPa. Chem Phys 2000;258(2-3):121-137.

[58] Ryckaert JP, Bellemans A. Molecular dynamics of liquid alkanes. Faraday Discuss 1978;66:95-106.

[59] Gyawali G, Sternfield S, Kumar R, Rick SW. Coarse-Grained Models of Aqueous and Pure Liquid Alkanes. J Chem Theor Comput 2017;13(8):3846-53.

[60] Vicent-Luna JM, Gutiérrez-Sevillano JJ, Hamad S, Anta J, Calero S. Role of Ionic Liquid [EMIM]+[SCN]− in the Adsorption and Diffusion of Gases in Metal–Organic Frameworks. ACS Appl Mater Interfaces 2018;10(35):29694-704.

[61] Rahman S, Lobanova O, Jiménez-Serratos G, Braga C, Raptis V, Muller EA, Jackson G, Avendano C, Galindo A. SAFT-γ Force Field for the Simulation of Molecular Fluids. 5. Hetero-Group Coarse-

Grained Models of Linear Alkanes and the Importance of Intramolecular Interactions. J Phys Chem B 2018.

[62] Xu RG, Xiang Y, Leng Y. Computational simulations of solvation force and squeezing out of dodecane chain molecules in an atomic force microscope. J Chem Phys 2017;147(5):054705.

[63] Edberg R, Evans DJ, Morriss GP. Constrained molecular dynamics: Simulations of liquid alkanes with a new algorithm. J Chem Phys 1986;84(12):6933-9.

[64] Zhao J, Yao G, Ramisetti SB, Hammond RB, Wen D. Molecular Dynamics Simulation of the Salinity Effect on the n-Decane/Water/Vapor Interfacial Equilibrium. Energy Fuels 2018.

[65] Fenter P, Geissbühler P, DiMasi E, Srajer G, Sorensen L B, Sturchio NC. Surface speciation of calcite observed in situ by high-resolution X-ray reflectivity. Geochim Cosmochim Acta 2000;64(7):1221-1228.

[66] Kerisit S, Parker SC. Free energy of adsorption of water and calcium on the {1014} calcite surface. Chem Commun 2004;1:52-53.

[67] Vasconcelos IF, Bunker BA, Cygan RT. Molecular dynamics modeling of ion adsorption to the basal surfaces of kaolinite. J Phys Chem C 2007;111(18):6753-6762.

[68] Chowdhuri S, Chandra A. Molecular dynamics simulations of aqueous NaCl and KCl solutions: Effects of ion concentration on the single-particle, pair, and collective dynamical properties of ions and water molecules. J Chem Phys 2001;115(8):3732-3741.

[69] Cooke DJ, Gray RJ, Sand KK, Stipp SL, Elliott JA. Interaction of ethanol and water with the {1014} surface of calcite. Langmuir 2010;26(18):14520-14529.

[70] Rajam S, Mann S. Selective stabilization of the (001) face of calcite in the presence of lithium. J Chem Soc Chem Comm 1990;1(24):1789-91.